Evaluation of Factors Influencing Changes in Land Surface Temperature at Gas Flaring Sites in the Niger Delta, Nigeria

Morakinyo, Barnabas Ojo[1,2,3,4*], Lavender, Samantha[2,3] & Abbott, Victor[2]
[1] Department of Surveying & Geoinformatics, Faculty of Environmental Sciences, BAZE University, Abuja, NIGERIA
[2]School of Marine Science & Engineering, Faculty of Science & Technology, University of Plymouth, Plymouth, UK
[3]Pixalytics Ltd, 1 Davy Rd, Tamar Science Park, Plymouth, UK
[4]ARGANS Ltd, 1 Davy Rd, Tamar Science Park, Plymouth, UK

*Corresponding author: Barnabas O. Morakinyo
E-mail: barnabas.ojo@bazeuniversity.edu.ng
Phone Number: +234 8103676990

Abstract
This research investigates factors that can affect changes in Land Surface Temperature (LST) retrieved from satellites data at 11 gas flaring sites in Rivers State, Nigeria. 8 Landsat 5 Thematic Mapper (TM), 22 Landsat 7 Enhanced Thematic Mapper Plus (ETM+), and 4 Landsat 8 Operational Land Imager and Thermal Infrared Sensor (OLI-TIRS) data from 14/12/1984 to 05/02/2022 with < 3 % cloud cover were used. LST was derived from the atmospherically corrected thermal band; difference between vegetation LST at 60m from the flare stack and vegetation LST at 450m from the flare stack was computed as ($\delta LST_{60\text{-}450m}$). Available factors that can affect ($\delta LST_{60\text{-}450m}$) considered are facility size, flare stack height and time. Pairwise linear regression analysis was applied to the relationship between each of the factor considered and ($\delta LST_{60\text{-}450m}$) in North, East, South, and West directions with $\alpha = 0.01$ to obtain r-values and p-values. Analysis of the relationships among multiple variables (x_1 = month, x_2 = facility size and x_3 = stack height, $y_1 = (\delta LST_{60\text{-}450mN})$ and $y_2 = (\delta LST_{60\text{-}450mE})$ was carried out using multiple linear regression analysis. The results ($r^2 = 0.05$, and p-value $= 0.016$) show that only 5 % of the variability in ($\delta LST_{60\text{-}450m}$) could be accounted for by the variables considered. From these results, it can be concluded that facility size, flare stack height and time could only account for 5 % of the variability in ($\delta LST_{60\text{-}450m}$) at the flaring sites examined.

Keywords: **Evaluation, Factors, Satellites data, Landsat, Land Surface Temperature.**

Introduction
The role of Land Surface Temperature (LST) in heat and energy exchange between land surfaces and the atmosphere is of great significance (Bechtel, 2015; Sun et al., 2011). The knowledge of LST is a bedrock for others Earth sciences system (Li et al., 2013; Kerr et al., 2000). For example, LST was used for detection of gas flares platforms (Morakinyo et al., 2021; Morakinyo et al., 2020), examination of urban heat island (Anastasios et al., 2018), soil moisture (Zhao et al., 2016), evapotranspiration (Song et al., 2018a), evaluation of environmental changes (Song et al., 2018b), climatic change analysis (Chapin et al., 2005), and geothermal area detection (Qin et al., 2011).

Some researchers have studied gas flaring temperatures globally as a strategy for discriminating gas flares hotspots from forest fires, bush burning and others using various Earth Observation (EO) satellites data. For example, the gas flaring temperatures of (1000-2600) K was derived from the Visible Infrared Imaging Radiometer Suite (VIIRS) Nightfire database by Liu et al. (2018) and Elvidge et al. (2016) derived. Caseiro et al. (2020) reported (1200-2500) K as gas

flares temperatures from shortwave and mid-infrared (SWIR and MIR) channels of Sentinel-3A Sea and Land Surface Temperature Radiometer (SLSTR) data. In addition, Elvidge et al. (2013) observed temperatures ranges of (1200-1750) K from VIIRS data. Furthermore, Zhang et al. (2015) and Elvidge et al. (2016) recorded (1450-2200) K as the radiant temperature retrieved from VIIRS data for the flaring sites investigated. A typical flaring site in the Niger Delta is shown in Figure 1.

Figure 1: Flare site in the Niger Delta; Source: (Edu, 2021).

In Nigeria, limited studies have been carried out on measurement of gas flaring temperatures whether by remote sensing technology (Morakinyo et al., 2022; Morakinyo et al., 2021; Morakinyo et al., 2020; Morakinyo, 2015) or conventional method (Morakinyo, 2015; Ubani and Onyejekwe, 2013; Dung et al., 2008). Specifically, no paper has been published on the examination of factors that can influence changes in LST retrieved from EO satellites at flaring sites in the Niger Delta. In addition, methods considered have not been used in any prior research for the Nigeria. Consequently, in order to close this gap the examination of the available factors that can influence changes in LST; and the application of remote sensing technology are required for the study. Research questions considered for this paper are: (1). What are the available factors (parameters) that can influence changes in LST at gas flaring sites in the Niger Delta? (2). What is the quantitative analysis of the relationship between each of the available parameter considered and the changes in LST in the North, East, South, and West directions? (3) What is the % contribution of the examined parameters to the changes in LST? Based on these 3 questions, the aim of the study is to evaluate factors that can influence changes in LST at the flaring sites in the Niger Delta and their % of contribution. Therefore, the definite objectives for the research questions are: (1) Selection of suitable flaring sites in the Niger Delta; (2) Retrieval of LST from atmospherically corrected Landsat 5 Thematic Mapper (TM), Landsat 7 Enhanced Thematic Mapper Plus (ETM+), and Landsat 8 Operational Land Imager (OLI) and Thermal Infrared Sensor (TIRS) data; (3) Computation of changes in LST as ($\delta LST_{60\text{-}450m}$) in North, East, South and West directions; (4) Application of pairwise and multiple linear regression of statistical analyses to the relationship between each of the available parameter and ($\delta LST_{60\text{-}450m}$) in the N, E, S and W directions.

Materials and Methods

Study Area

This research was conducted with 11 oil and gas facilities flaring sites located in Rivers State, Niger Delta of Nigeria. The study area is bounded by Latitude 4° 40′ and 5° 01′ N and Longitude 6° 50′ and 7° 01′ E (Morakinyo et al., 2021). The name and dimension of the facility within each site is Eleme Petroleum Refinery Companies I (1.6 × 1.1) km; and II (2.2 × 1.3)

km; Bonny Liquefied Natural Gas (LNG) plant (4.2 × 2.8) km; Onne (175 × 130) m; Rukpokwu (350 × 350) m; Umurolu (4.2 × 2.4) km; Obigbo (650 × 650) m; Alua (170 × 90) m; Umudioga (100 × 100) m and Chokocho (350 × 120) m Flow Stations, and Sara oil well (350 × 250) m (Figures 2 and 3A). The height of the flare stack for each of the facility is presented in Figure 3B. Among the 11 sites studied, Bonny LNG and Sara oil well are located at coastal areas that are not accessible by road; while the rest of the 9 are inland facilities. In order to explore the LST results for adequate analysis, (12 × 12) km area was examined around the flare stacks.

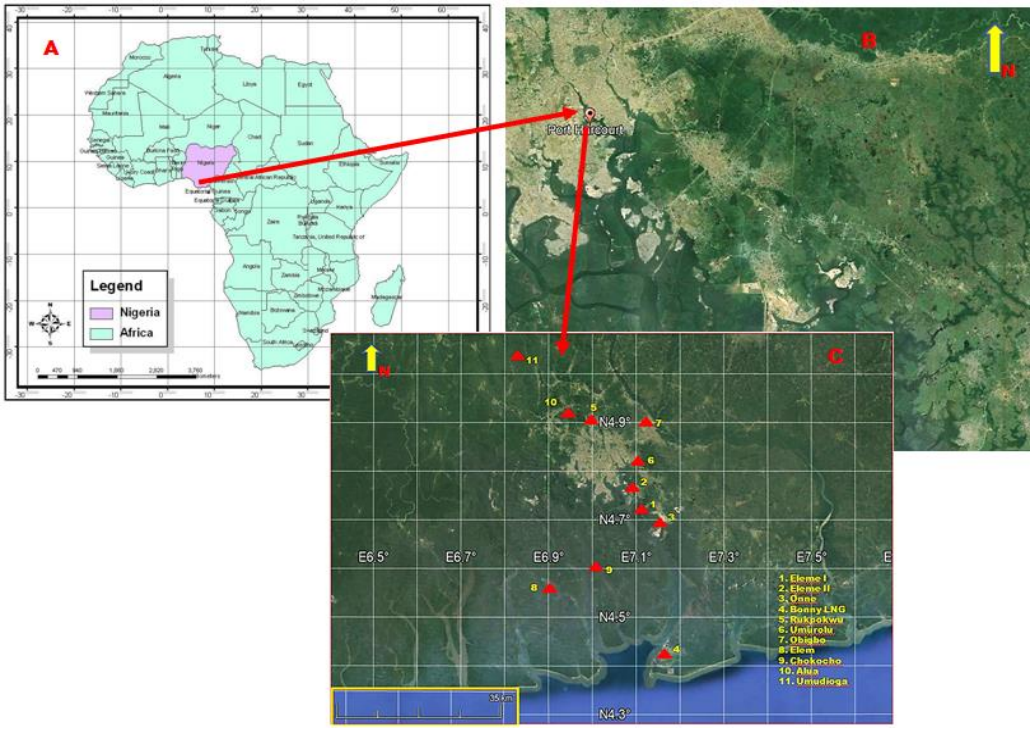

Figure 2: A) Map of Africa showing Nigeria, (ESRI, 2022); B) Location of Rivers State in the Niger Delta, Nigeria (Google Earth, 2022); C) The 11 flaring sites studied in Rivers State, Nigeria.

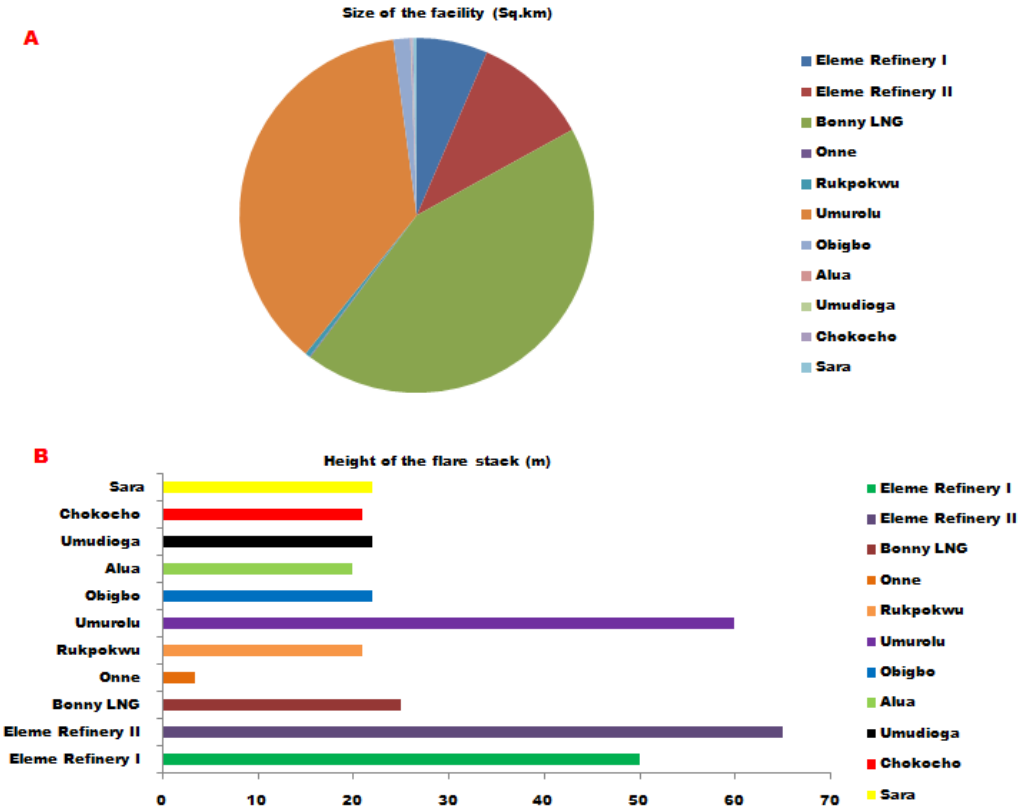

Figure 3: A) Size of the 11 facilities; B) Height of the flare stack for the 11 facilities

Data and Processing Methods using MATLAB Programming Codes

Data used in this research are Landsat 5 TM, Landsat 7 ETM+, Landsat 8 OLI-TIRS, and high resolution images from IKONO. 8 Landsat 5 TM imagery dated 1984 to 1991; 22 Landsat 7 ETM+ imagery dated 1999 to 2013; and 4 Landsat 8 OLI-TIRS data dated 2018 to 2022 with < 3 % cloud cover from the months of January to April, and November to December acquired from the USGS Earth Resources Observation and Science (EROS) Data Centre website (http://earthexplorer.usgs.gov/) were used. The datasets were selected because they are less affected by clouds and that they fall within the dry season in Nigeria. The spatial resolution for Landsat 5 and Landsat 7 band 6 (Thermal Infrared) are 120 m and 60 m respectively while that of Landsat 8 OLI-TIRS bands 10 and 11 (Thermal Infrared) is 100 m but all are resampled to 30m pixels (USGS, 2022; Chander and Markham, 2003).

Landsat 5 and Landsat 7 thermal band Digital Numbers (DN) values were processed to top of atmosphere (TOA) spectral radiance with equation 1 using MATLAB codes.

$L_\lambda = ((LMAX_\lambda - LMIN_\lambda)/(QCALMAX - QCALMIN)) * (QCAL-QCALMIN) + LMIN_\lambda$ (Eq. 1)

Where:

$L_\lambda =$ Spectral radiance at the sensor's aperture ($Wm^{-2}sr^{-1}\mu m^{-1}$);

QCAL = The quantized calibrated pixel value in DN;

$LMIN_\lambda =$ The spectral radiance that is scaled to QCALMIN ($Wm^{-2}sr^{-1}\mu m^{-1}$);

$LMAX_\lambda =$ The spectral radiance that is scaled to QCALMAX ($Wm^{-2}sr^{-1}\mu m^{-1}$);

QCALMIN = The minimum quantized calibrated pixel value (corresponding to $LMIN_\lambda$) in DN = 1 for LPGS (a processing software version) products;

QCALMAX = The maximum quantized calibrated pixel value (corresponding to $LMAX_\lambda$) in DN = 255.

Also, the spectral reflectance for Landsat 5 and Landsat 7 multispectral bands (1-4); and bands 2-5 for Landsat 8 were computed using (Eq. 2) (Song et al., 2018a).

$$\boldsymbol{\rho}_p = (\boldsymbol{\pi} \times L_\lambda \times d^2) \div (ESUN_\lambda \times Cos\boldsymbol{\theta s}) \quad \text{(Eq. 2)}$$

Where: $\rho p =$ Unitless effective at-satellite planetary reflectance;
$L =$ is measured per unit solid angle;
$\boldsymbol{\pi}L =$ Upwelling radiance over a full hemisphere;
$d =$ Earth-Sun distance in astronomical units;
$ESUN_\lambda =$ Mean solar exoatmospheric irradiances;
$\theta s =$ Solar zenith incident angle in degrees.

Application of K-means Function of MATLAB

The unsupervised cluster analysis (Morakinyo et al., 2019) of the Landsat 5 and Landsat 7 atmospherically corrected reflectance (bands 1-4), and that of Landsat 8 OLI-TIRS (bands 2-5) using the k-means function of MATLAB for land cover (LC) classification was carried out for all the sites to obtain 4 classes of LC (vegetation, soil, built up and water) (Maaharjan, 2018) (Figure 4). The % of each of the LC type were identified at the study sites during ground validation fieldwork from 04/08/2012-21/09/2012 and 05/08/2020- 21/09/2020. Red, Green, Blue (RGB) pseudo-true colour composite images, high resolution images from Google Earth, and Digital Global were used for further clarifications of the 4 LC types.

The emissivity (ε) value for the 4 LC types available at each site is obtained by considering the ε value of each of the LC type on pixel basis for the entire site. Minimum and maximum ε values were acquired from the literature for the computation of the mean ε values for the 4 LC types for each pixel with the % of each LC within a pixel applied (Morakinyo et al., 2021; Morakinyo et al., 2019). Consequently, the ε value for a Landsat pixel's LC is a combination of the ε value of all the 4 LC types present within the pixel.

Landsat LST Retrieval

The retrieval of LST from Landsat data was carried out using radiative transfer equation. This method has 3 stages (Zhang et al., 2009; Yuan and Bauer, 2007). Stage 1 is to convert the DN of thermal bands to TOA radiance using (1) for Landsat 5 and Landsat 7 data. For Landsat 8 images, TIRS band data can be converted to TOA spectral radiance using (Eq. 3).

$$L_\lambda = M_L * QCAL + A_L \quad \text{(Eq. 3)}$$

Where:
$M_L =$ The band specific multiplicative rescaling factor;
$A_L =$ The band specific additive rescaling factor.
M_L and A_L are provided in the metadata file of the Landsat 8 data. L_λ and QCAL in (3) are the same as those in (1). Conversion of TOA radiance of the thermal band to surface-leaving radiance using the atmospheric correction tool MODTRAN 4.1 to remove the effects of the atmosphere (Berk et al., 1999) is the stage 2. The surface-leaving radiance L_T is calculated using (Eq. 4) (Barsi et al., 2005).

$$L_T = (L_\lambda - L_\mu - \tau\,(1-\varepsilon)L_d)/\tau\varepsilon \quad \text{(Eq. 4)}$$

Where L_μ, L_d and τ, are the upwelling radiance, downwelling radiance, and atmospheric transmission respectively; and they are atmospheric correction parameters for the Landsat thermal band. ε is the emissivity of the surface LC types. For this study, ε was calculated based

on the land cover types of each site. Stage 3 is the conversion of radiance to LST using the Landsat-specific estimate of the Planck curve (Eq. 5) (Chander, and Markham, 2003):

$$LST = \frac{K_2}{\ln((K_1/L_\lambda) + 1)} \qquad \text{(Eq. 5)}$$

Where:
LST = Temperature in Kelvin (K) (Figure 4); K_1 and K_2 are thermal band calibration constants calculated for the Landsat sensor characteristics (Table 1).

Table 1: Calibration Constants K_1 and K_2 for Landsat 5 TM, Landsat 7 ETM+ and Landsat 8 TIRS data

	Landsat 5 TM	Landsat 7 ETM+	Landsat 8 Band 10	Landsat 8 Band 11
K_1 ($Wm^{-2}sr^{-1}\mu m^{-1}$)	607.76	666.09	774.89	480.89
K_2 (K)	1260.56	1282.71	1321.08	1201.14

Source: (USGS, 2022)

Large uncertainty in the band 11 values for Landsat 8 were recorded at the product information on 14/11/2013 (http://landsat.usgs.gov/Landsat8_Using_Product.php); and so, using band 10 data to retrieve LST was recommended. Hence, for Landsat 8, band 10 data while for Landsat 5 and Landsat 7 band 6 data were used for the retrieval of LST accordingly. LST were determined for all the 4 (Vegetation, soil, built up, and water) LC types present at the 11 study sites.

Computation of Change in LST for Vegetation as ($\delta LST_{60\text{-}450m}$)

LST for vegetation was used for further study, hence changes in LST for vegetation was computed as ($\delta LST_{60\text{-}450m}$) which is the difference between the LST for vegetation at 60 m distance from the flare stack and the LST for vegetation at 450 m distance from the flare stack (Morakinyo, 2015). The 60 m was chosen and used for the pixel after the flare stack to know the LST for vegetation at a near distance from the flare. Also, 450 m was adopted as a far distance from the flare; and this is supported by Dung et al. (2008) and Isichei and Sandford (1976) that the maximum distance of the impact of flare on vegetation is between 100 to 120 m.

i.e. $LST_{60} - LST_{450m} = (\delta LST_{60\text{-}450m})$ (Eq. 6)

($\delta LST_{60\text{-}450m}$) was applied to each of the available factor that can influence it; and the relationship between them in the N, E, S and W directions were examined for the purpose of this study.

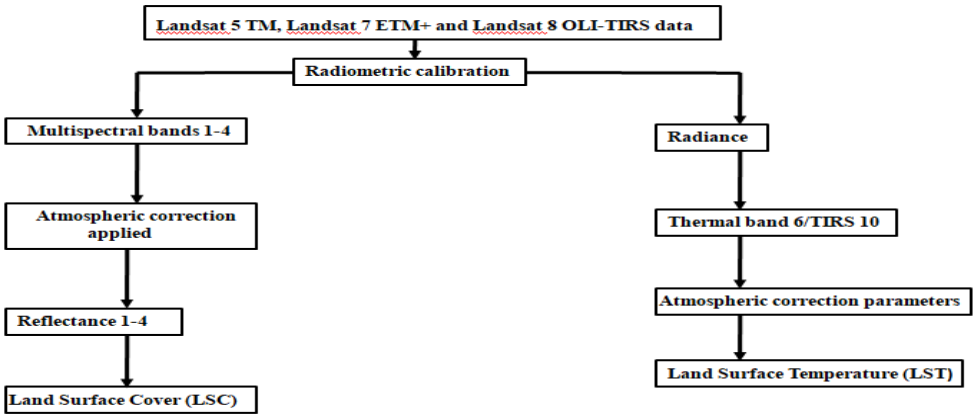

Figure 4: Flowchart showing the stages for the processing of Landsat 5, Landsat 7 and Landsat 8 data for land cover classification and LST retrieval.

Factors that can Influence ($\delta LST_{60\text{-}450m}$) at Flaring Sites in the Niger Delta

Factors that can impact ($\delta LST_{60\text{-}450m}$) at flaring sites in the Niger Delta include volume and rate of the burning gas, facility size, flare stack height, vegetation type and density, and time (Julian day, month and year). However, those 3 factors that cannot be derived from satellite data and are available and investigated for this study are facility size, stack height and time (Julian day, month and year).

Size of the facility is considered in order to compare the results ($\delta LST_{60\text{-}450m}$) obtained from various oil and gas facilities of different sizes ranging from small, medium to large. For example, comparing results obtained from Eleme Refinery II, Bonny LNG and Sara oil well. Height of the flare stack helps to evaluate the impact of the height of the stack on the $\delta LST_{60\text{-}450m}$, since the height of the flare stacks of all the facilities considered are not equal, as well as the location of some of the facilities is different (Coastal and inland). Similarly, time which is the acquisition date (Julian day, month and year) for the acquired Landsat data is considered in order to assess the effect of the period of satellite observation on ($\delta LST_{60\text{-}450m}$).

Analysis of Variance (ANOVA): Determination of r-values, p-values and Correlation Type

To establish the reliability on ($\delta LST_{60\text{-}450m}$) as a true measure of flare impact, an analysis of variance (ANOVA) was carried out to test whether both near and far temperatures from the flare were significantly different (with $\alpha = 0.01$). Linear relationships between each of the 3 factors and ($\delta LST_{60\text{-}450m}$) were tested against the North, East, South and West directions, and it give better results. Furthermore, the pairwise linear regression analysis was applied to the relationships between each of the factors considered and ($\delta LST_{60\text{-}450m}$) in the N, E, S and W directions with $\alpha = 0.01$ to give the first set of correlation coefficients (r-values and p-values) (Table 18). Also, Table 19 presented the second set of r-values and p-values determined with a condition that ($\delta LST_{60\text{-}450m}$) with a p-value $> \alpha = 0.01$ should not be considered for the computation.

Investigation with Multiple Linear Regression

The purpose of multiple linear regression analysis is to analyze relationships among multiple variables. The analysis is carried out through the estimation of a relationship $y = f(x_1, x_2, ..., x_k)$ and the results serve the following purposes:

(1) Answer the question of how much y changes with changes in each $x(x_1, x_2, ..., x_k)$, and
(2) Predict the value of y based on the x values.

For this research, $x_1 =$ Month, $x_2 =$ Facility size and $x_3 =$ Flare stack height.
$y_1 = \delta LST_{fs\text{-}450mN}$ and $y_2 = \delta LST_{fs\text{-}450mE}$.
$x_1, x_2, x_3 =$ Predictor variables.
$y_1, y_2 =$ Response variables.
Each variable is standardized as shown in equations 8-10. Generally, the linear model for multiple regressions is:

$$y = bx \quad \text{(Eq. 7)}$$

Where b = Relative quantitative contribution of each x predictor variable

$$\text{Month} = [\text{month} - (\text{meanmonth})] \div \sigma_{\text{month}} \quad \text{(Eq. 8)}$$

$$\text{Facility size} = [\text{facility size} - (\text{meanfacility size})] \div \sigma_{\text{facility size}} \quad \text{(Eq. 9)}$$

$$\text{Flare stack height} = [\text{flare stack height} - (\text{meanflare stack height})] \div \sigma_{\text{stack height}} \quad \text{(Eq. 10)}$$

For this research, (Eq. 7) has become the following:
For y_1,

$$\delta LST_{fs\text{-}450mN} = b_o + b_1 \times (\text{Month}) + b_2 \times (\text{Facility size}) + b_3 \times (\text{Flare stack height}) \quad \text{(Eq. 11)}$$

For y_2,

$\delta LST_{fs\text{-}450mE} = b_o + b_1 \times (\text{Month}) + b_2 \times (\text{Facility size}) + b_3 \times (\text{Flare stack height})$ (Eq. 12)

Where,

b_o = constant.

Results and Discussion

Landsat LST Retrieval and Computation of Change in LST as $\delta LST_{60\text{-}450m}$

LST's for vegetation, soil, built up and water were determined for all the 11 sites examined (Eq.5). The computed changes in LST for vegetation ($\delta LST_{60\text{-}450m}$) (Eq. 6) in the N, E, S and W directions for 1990, 2000, 2010 and 2022 are presented in Tables 2-17.

Table 2: ($\delta LST_{60\text{-}450m}$) (K) (North direction, 1990)

Site	LST (K) at 60 m	LST (K) at 450 m	($\delta LST_{60\text{-}450m}$) (K)
Eleme Refinery I	317	284	33
Eleme Refinery II	320	286	34
Onne	317	274	43
Umurolu	318	290	28
Bonny LNG	358	301	57
Alua	350	304	46
Rukpokwu	334	298	36
Obigbo	337	307	30
Chokocho	345	305	40
Umudioga	319	290	29
Sara	333	300	33

Table 3: ($\delta LST_{60\text{-}450m}$) (K) (East direction, 1990)

Site	LST (K) at 60 m	LST (K) at 450 m	($\delta LST_{60\text{-}450m}$) (K)
Eleme Refinery I	324	286	38
Eleme Refinery II	316	280	36
Onne	320	286	34
Umurolu	308	287	21
Bonny LNG	322	289	33
Alua	343	311	32
Rukpokwu	313	280	33
Obigbo	330	300	30
Chokocho	323	287	36
Umudioga	312	276	36
Sara	321	282	39

Table 4: ($\delta LST_{60\text{-}450m}$) (K) (South direction, 1990)

Site	LST (K) at 60 m	LST (K) at 450 m	($\delta LST_{60\text{-}450m}$) (K)
Eleme Refinery I	322	285	37
Eleme Refinery II	312	278	34
Onne	314	280	34
Umurolu	306	273	33
Bonny LNG	320	285	35
Alua	335	298	37
Rukpokwu	317	279	38
Obigbo	323	289	34
Chokocho	315	276	39
Umudioga	306	273	33
Sara	313	281	32

Table 5: ($\delta LST_{60\text{-}450m}$) (K) (West direction, 1990)

Site	LST (K) at 60 m	LST (K) at 450 m	($\delta LST_{60\text{-}450m}$) (K)
Eleme Refinery I	310	275	35
Eleme Refinery II	328	283	45
Onne	308	265	43
Umurolu	304	268	36
Bonny LNG	327	292	35
Alua	327	288	39
Rukpokwu	324	283	41
Obigbo	327	291	36
Chokocho	330	290	40
Umudioga	313	278	35
Sara	317	286	31

Table 6: ($\delta LST_{60\text{-}450m}$) (K) (North direction, 2000)

Site	LST (K) 60 m	LST (K) at 450 m	($\delta LST_{60\text{-}450m}$) (K)
Eleme Refinery I	325	286	39
Eleme Refinery II	328	278	50
Onne	324	271	53
Umurolu	313	272	41
Bonny LNG	350	283	67
Alua	357	286	71
Rukpokwu	329	283	46
Obigbo	344	284	60
Chokocho	347	288	59
Umudioga	326	280	46
Sara	337	295	42

Table 7: ($\delta LST_{60\text{-}450m}$) (K) (East direction, 2000)

Site	LST (K) at 60 m	LST (K) at 450 m	($\delta LST_{60\text{-}450m}$) (K)
Eleme Refinery I	326	286	40
Eleme Refinery II	327	280	47
Onne	320	267	53
Umurolu	320	273	47
Bonny LNG	339	286	53
Alua	352	292	60
Rukpokwu	323	280	43
Obigbo	340	291	49
Chokocho	332	286	46
Umudioga	322	279	43
Sara	330	281	49

Table 8: ($\delta LST_{60\text{-}450m}$) (K) (South direction, 2000)

Site	LST (K) at 60 m	LST (K) at 450 m	($\delta LST_{60\text{-}450m}$) (K)
Eleme Refinery I	331	281	50
Eleme Refinery II	330	275	55
Onne	321	270	51
Umurolu	325	266	59
Bonny LNG	339	281	58
Alua	351	287	64
Rukpokwu	326	281	45
Obigbo	340	288	52
Chokocho	333	279	54
Umudioga	325	280	45
Sara	330	278	52

Table 9: ($\delta LST_{60\text{-}450m}$) (K) (West direction, 2000)

Site	LST (K) at 60 m	LST (K) at 450 m	($\delta LST_{60\text{-}450m}$) (K)
Eleme Refinery I	331	296	35
Eleme Refinery II	325	289	36
Onne	311	271	40
Umurolu	322	284	38
Bonny LNG	334	296	38
Alua	336	299	37
Rukpokwu	325	290	35
Obigbo	335	295	40
Chokocho	332	297	35
Umudioga	321	291	30
Sara	327	293	34

Table 10: ($\delta LST_{60\text{-}450m}$) (K) (North direction, 2010)

Site	LST (K) at 60 m	LST (K) at 450 m	($\delta LST_{60\text{-}450m}$) (K)
Eleme Refinery I	329	295	34
Eleme Refinery II	332	287	45
Onne	324	271	53
Umurolu	330	287	43
Bonny LNG	349	300	49
Alua	358	293	65
Rukpokwu	336	300	36
Obigbo	346	298	48
Chokocho	352	300	52
Umudioga	341	285	56
Sara	340	292	48

Table 11: ($\delta LST_{60\text{-}450m}$) (K) (East direction, 2010)

Site	LST (K) at 60 m	LST (K) at 450 m	($\delta LST_{60\text{-}450m}$) (K)
Eleme Refinery I	340	296	44
Eleme Refinery II	338	290	48
Onne	328	276	52
Umurolu	334	287	47
Bonny LNG	342	299	43
Alua	354	301	53
Rukpokwu	331	291	40
Obigbo	342	300	42
Chokocho	340	298	42
Umudioga	338	286	52
Sara	335	294	41

Table 12: ($\delta LST_{60\text{-}450m}$) (K) (South direction, 2010)

Site	LST (K) at 60 m	LST (K) at 450 m	($\delta LST_{60\text{-}450m}$) (K)
Eleme Refinery I	331	298	33
Eleme Refinery II	323	287	36
Onne	301	270	31
Umurolu	317	281	36
Bonny LNG	328	296	32
Alua	331	294	37
Rukpokwu	325	293	32
Obigbo	334	296	38
Chokocho	340	295	45
Umudioga	317	284	33
Sara	325	298	27

Table 13: ($\delta LST_{60\text{-}450m}$) (K) (West direction, 2010)

Site	LST (K) at 60 m	LST (K) at 450 m	($\delta LST_{60\text{-}450m}$) (K)
Eleme Refinery I	328	291	37
Eleme Refinery II	326	284	42
Onne	308	266	42
Umurolu	320	282	38
Bonny LNG	331	291	40
Alua	330	294	36
Rukpokwu	321	285	36
Obigbo	332	295	37
Chokocho	328	292	36
Umudioga	320	293	27
Sara	327	287	40

Table 14: ($\delta LST_{60\text{-}450m}$) (K) (North direction, 2022)

Site	LST (K) at 60 m	LST (K) at 450 m	($\delta LST_{60\text{-}450m}$) (K)
Eleme Refinery I	343	298	45
Eleme Refinery II	339	292	47
Onne	327	278	49
Umurolu	336	290	46
Bonny LNG	348	301	47
Alua	354	303	51
Rukpokwu	337	279	58
Obigbo	349	294	55
Chokocho	343	301	42
Umudioga	335	291	44
Sara	340	293	47

Table 15: ($\delta LST_{60\text{-}450m}$) (K) (East direction, 2022)

Site	LST (K) at 60 m	LST (K) at 450 m	($\delta LST_{60\text{-}450m}$) (K)
Eleme Refinery I	331	298	33
Eleme Refinery II	329	287	42
Onne	319	271	48
Umurolu	325	280	45
Bonny LNG	338	289	49
Alua	342	285	57
Rukpokwu	322	283	39
Obigbo	338	292	46
Chokocho	331	285	46
Umudioga	326	274	52
Sara	324	281	43

Table 16: ($\delta LST_{60\text{-}450m}$) (K) (South direction, 2022)

Site	LST (K) at 60 m	LST (K) at 450 m	($\delta LST_{60\text{-}450m}$) (K)
Eleme Refinery I	338	297	41
Eleme Refinery II	331	289	42
Onne	318	272	46
Umurolu	330	284	46
Bonny LNG	342	295	47
Alua	341	297	44
Rukpokwu	335	291	44
Obigbo	343	294	49
Chokocho	346	292	54
Umudioga	330	290	40
Sara	336	291	45

Table 17: ($\delta LST_{60\text{-}450m}$) (K) (West direction, 2022)

Site	LST (K) at 60 m	LST (K) at 450 m	($\delta LST_{60\text{-}450m}$) (K)
Eleme Refinery I	344	297	47
Eleme Refinery II	338	289	49
Onne	324	268	56
Umurolu	340	283	57
Bonny LNG	347	294	53
Alua	349	298	51
Rukpokwu	338	291	47
Obigbo	348	300	48
Chokocho	345	298	47
Umudioga	334	281	53
Sara	340	300	40

Relationship between Factors that can Influence LST and ($\delta LST_{60\text{-}450m}$) in the North, East, South and West Directions

Analysis of ANOVA was used to obtain the results presented in Tables 18 and 19 which show the results of the first and second sets of the values of r and that of p, and the correlation type that resulted from the relationship between each of the facility size, the flare stack height and the time, and ($\delta LST_{60\text{-}450m}$) in the N, E, S and W directions. The range of p-values and that of the ($\delta LST_{60\text{-}450m}$) obtained in the 4 cardinal directions are presented in Table 20. Furthermore, Figures 5-9 also show the graphical presentation of the results obtained from the relationship between each of the facility size, flare stack height, and time (Julian day, month and year) and that of ($\delta LST_{60\text{-}450m}$) in the N, E, S and W directions.

Table 18: First set of r and p values and their correlation type for the relationship between each of the factor considered and ($\delta LST_{60\text{-}450m}$) when $\alpha = 0.01$

Relationship	r-value	p-value	Correlation type
Facility size against ($\delta LST_{60\text{-}450m}$)$_N$	−0.191	**3.390×10^{-4}**	−
Facility size against ($\delta LST_{60\text{-}450m}$)$_E$	−0.202	**1.669×10^{-4}**	−
Facility size against ($\delta LST_{60\text{-}450m}$)$_S$	−0.180	**9.979×10^{-4}**	−
Facility size against ($\delta LST_{60\text{-}450m}$)$_W$	−0.152	**0.004**	−
Flare stack height against ($\delta LST_{60\text{-}450m}$)$_N$	−0.121	0.055	−
Flare stack height against ($\delta LST_{60\text{-}450m}$)$_E$	−0.103	0.131	−
Flare stack height against ($\delta LST_{60\text{-}450m}$)$_S$	0.470	0.028	+
Flare stack height against ($\delta LST_{60\text{-}450m}$)$_W$	−0.162	**0.012**	−
Julian day against ($\delta LST_{60\text{-}450m}$)$_N$	0.071	0.225	+
Julian day against ($\delta LST_{60\text{-}450m}$)$_E$	0.122	0.029	+
Julian day against ($\delta LST_{60\text{-}450m}$)$_S$	0.101	0.064	+
Julian day against ($\delta LST_{60\text{-}450m}$)$_W$	0.073	0.166	+
Month against ($\delta LST_{60\text{-}450m}$)$_N$	0.071	0.190	+
Month against ($\delta LST_{60\text{-}450m}$)$_E$	0.123	0.025	+
Month against ($\delta LST_{60\text{-}450m}$)$_S$	0.104	0.061	+
Month against ($\delta LST_{60\text{-}450m}$)$_W$	0.081	0.150	+
Year against ($\delta LST_{60\text{-}450m}$)$_N$	0.003	0.958	+
Year against ($\delta LST_{60\text{-}450m}$)$_E$	−0.004	0.947	−
Year against ($\delta LST_{60\text{-}450m}$)$_S$	−0.009	0.875	−
Year against ($\delta LST_{60\text{-}450m}$)$_W$	0.032	0.552	+

Table 19: Second set of r and p values and their correlation type for the relationship between each of the factor considered and ($\delta LST_{60\text{-}450m}$) when $\alpha = 0.01$

Relationship	r-value	p-value	Correlation type
Facility size against $(\delta LST_{60\text{-}450m})_N$	−0.182	**0.002**	−
Facility size against $(\delta LST_{60\text{-}450m})_E$	−0.202	**5.078×10^{-4}**	−
Facility size against $(\delta LST_{60\text{-}450m})_S$	−0.171	**0.003**	−
Facility size against $(\delta LST_{60\text{-}450m})_W$	−0.140	**0.020**	−
Flare stack height against $(\delta LST_{60\text{-}450m})_N$	−0.152	0.035	−
Flare stack height against $(\delta LST_{60\text{-}450m})_E$	−0.103	0.142	−
Flare stack height against $(\delta LST_{60\text{-}450m})_S$	−0.126	0.074	−
Flare stack height against $(\delta LST_{60\text{-}450m})_W$	−0.169	**0.019**	−
Julian day against $(\delta LST_{60\text{-}450m})_N$	0.101	0.088	+
Julian day against $(\delta LST_{60\text{-}450m})_E$	0.110	0.061	+
Julian day against $(\delta LST_{60\text{-}450m})_S$	0.113	0.050	+
Julian day against $(\delta LST_{60\text{-}450m})_W$	0.070	0.244	+
Month against $(\delta LST_{60\text{-}450m})_N$	0.105	0.078	+
Month against $(\delta LST_{60\text{-}450m})_E$	0.112	0.055	+
Month against $(\delta LST_{60\text{-}450m})_S$	0.115	0.047	+
Month against $(\delta LST_{60\text{-}450m})_W$	0.075	0.213	+
Year against $(\delta LST_{60\text{-}450m})_N$	−0.027	0.647	−
Year against $(\delta LST_{60\text{-}450m})_E$	−0.005	0.927	−
Year against $(\delta LST_{60\text{-}450m})_S$	−0.029	0.620	−
Year against $(\delta LST_{60\text{-}450m})_W$	0.043	0.479	+

Table 20: Limit of p-values and that of ($\delta LST_{60\text{-}450m}$) (K)

($\delta LST_{60\text{-}450m}$)	Limit of p-values	Limit of ($\delta LST_{60\text{-}450m}$) (K)
$(\delta LST_{60\text{-}450m})_N$	$\ll$ 0.00001-0.146	0.6-35.5 = 34.9
$(\delta LST_{60\text{-}450m})_E$	$\ll$ 0.00001-0.127	0.9-36.7 = 35.8
$(\delta LST_{60\text{-}450m})_S$	$\ll$ 0.00001-0.143	0.7-28.6 = 27.9
$(\delta LST_{60\text{-}450m})_W$	$\ll$ 0.00001-0.146	0.7-32.0 = 31.3

Multiple Linear Regression Analysis

The r^2, p-value, b_0, b_1, b_2 and b_3 results obtained from (Eq. 11) are:

$r^2 = 0.05$; $p = 0.016$;

$b_0 = \sim 0$; $b_1 = 0.09$; $b_2 = -0.146$; $b_3 = -0.103$.

Similarly, (Eq. 12) gives the following results,

$r^2 = 0.05$; $p = 0.011$;

$b_0 = \sim 0$; $b_1 = 0.069$; $b_2 = -0.195$; $b_3 = -0.053$.

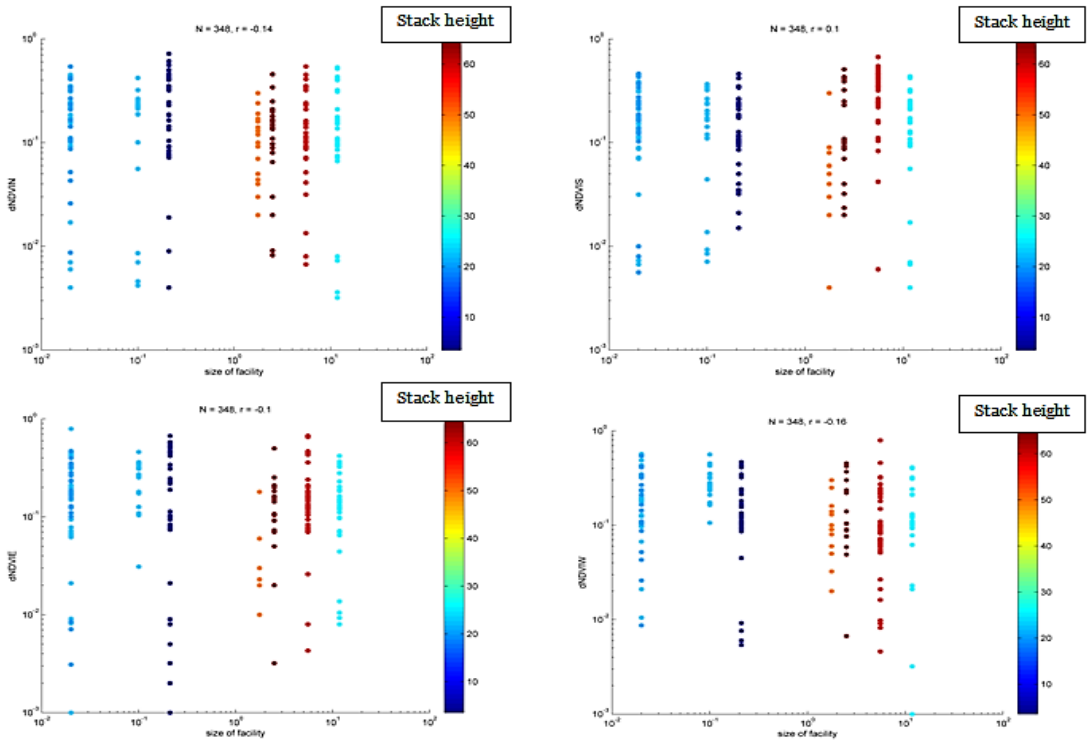

Figure 5: Facility size: Upper left) v ($\delta LST_{60\text{-}450m}$)$_N$; Lower left) v ($\delta LST_{60\text{-}450m}$)$_E$; Upper right) v ($\delta LST_{60\text{-}450m}$)$_S$; Lower right) v ($\delta LST_{60\text{-}450m}$)$_W$

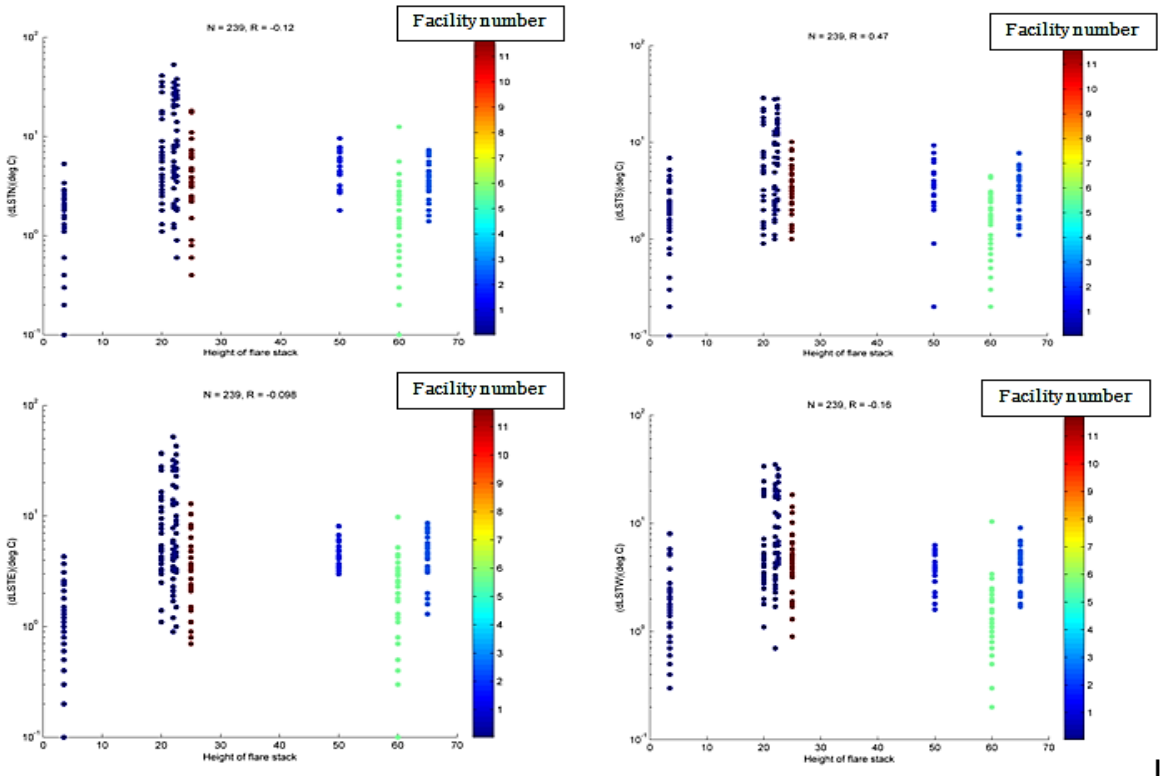

Figure 6: Flare stack height: Upper left) v ($\delta LST_{60\text{-}450m}$)$_N$; Lower left) v ($\delta LST_{60\text{-}450m}$)$_E$; Upper right) v ($\delta LST_{60\text{-}450m}$)$_S$; Lower right) v ($\delta LST_{60\text{-}450m}$)$_W$

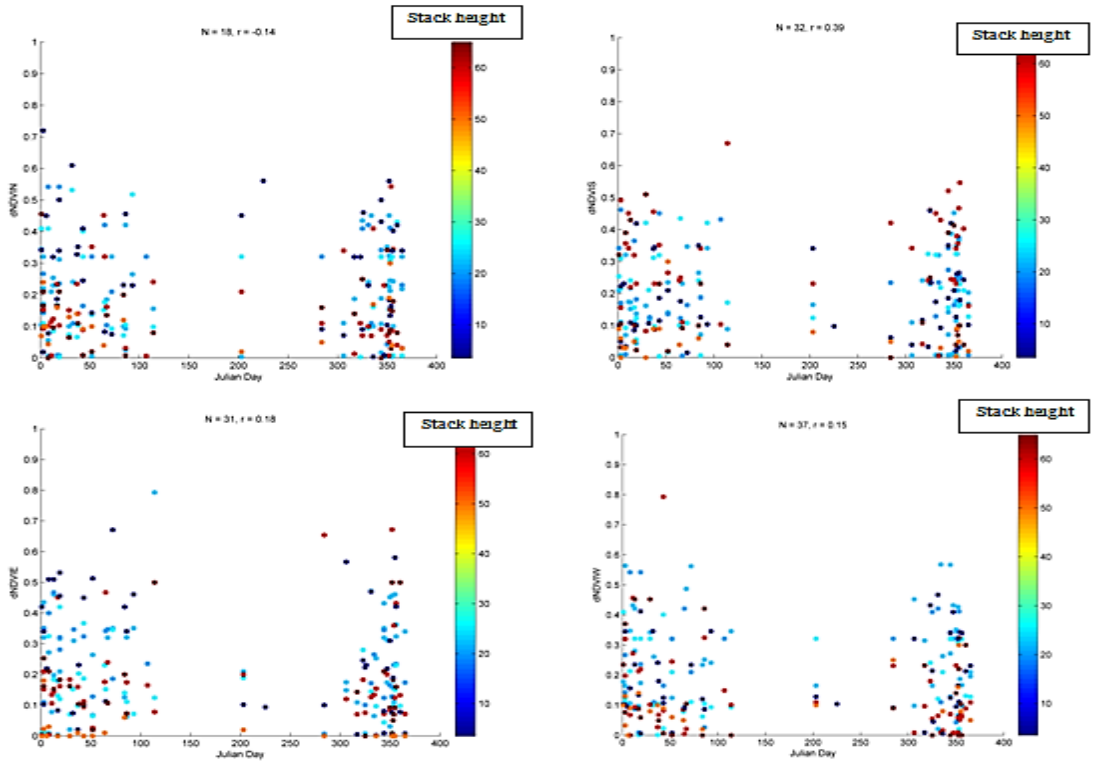

Figure 7: Julian day: Upper left) v ($\delta LST_{60-450m}$)$_N$; Lower left) v ($\delta LST_{60-450m}$)$_E$; Upper right) v ($\delta LST_{60-450m}$)$_S$; Lower right) v ($\delta LST_{60-450m}$)$_W$

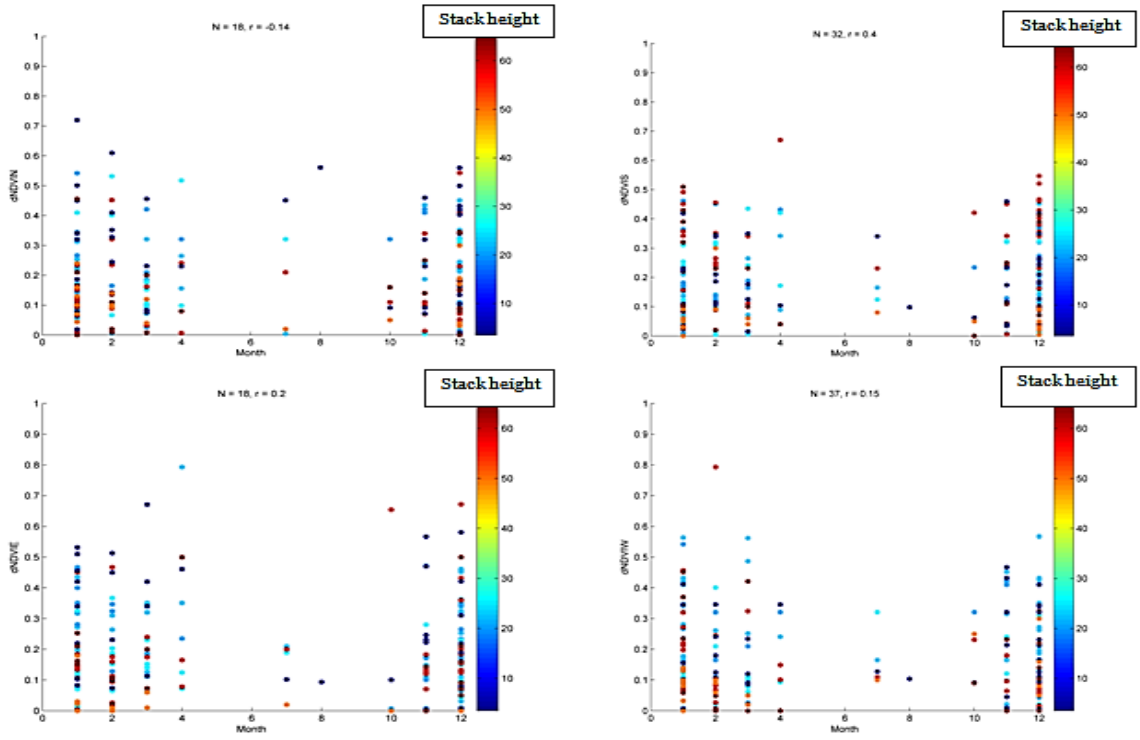

Figure 8: Month: Upper left) v ($\delta LST_{60-450m}$)$_N$; Lower left) v ($\delta LST_{60-450m}$)$_E$; Upper right) v ($\delta LST_{60-450m}$)$_S$; Lower right) v ($\delta LST_{60-450m}$)$_W$

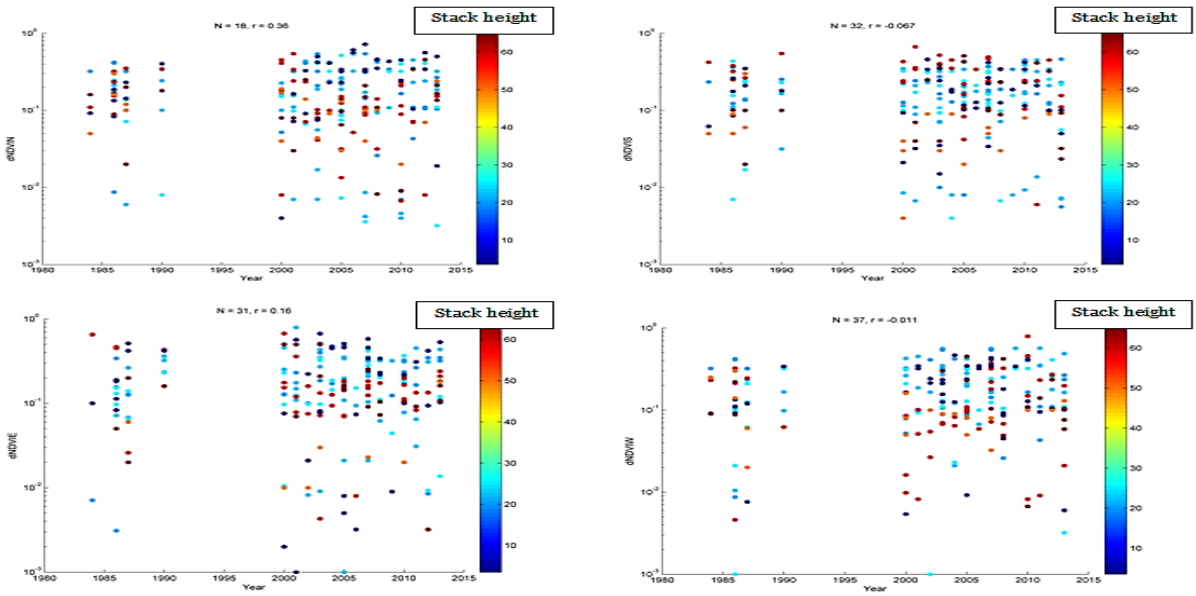

Figure 9: Year: Upper left) v ($\delta LST_{60\text{-}450m}$)$_N$; Lower left) v ($\delta LST_{60\text{-}450m}$)$_E$; Upper right) v ($\delta LST_{60\text{-}450m}$)$_S$; Lower right) v ($\delta LST_{60\text{-}450m}$)$_W$

The changes in vegetation LST ($\delta LST_{60\text{-}450m}$) (K) obtained for the study (Table 2-17) varies. This suggests that some factors are responsible for it, among which are the volumes and rates of the burning gas, vegetation type and density, time of satellite overpass etc. However, data on both the volumes and the rate of the burning gas are not available; and so their impacts on the results could not be accounted for.

In Tables 18 and 19, all relationships with significant impact are shown in bold. Table 20 show the range of p-values, and that of ($\delta LST_{60\text{-}450m}$) (K) in the N, E, S and W directions. The results obtained from the relationship of each of the factor considered with ($\delta LST_{60\text{-}450m}$) in the 4 cardinal directions are presented in Figures 5-9. For Figures 5, 7, 8 and 9, the colour bar represents the flare stack height but for Figure 6, the colour bar is representing the facility number.

In Table 18, the relationship between the facility size and each of the ($\delta LST_{60\text{-}450m}$)$_N$, ($\delta LST_{60\text{-}450m}$)$_E$, ($\delta LST_{60\text{-}450m}$)$_S$ and ($\delta LST_{60\text{-}450m}$)$_W$ give statistically significant results but negative correlation. For the flare stack height and each of the ($\delta LST_{60\text{-}450m}$)$_N$, ($\delta LST_{60\text{-}450m}$)$_E$ and ($\delta LST_{60\text{-}450m}$)$_W$, the relationship show negative correlation except ($\delta LST_{60\text{-}450m}$)$_S$ that show positive correlation. The p-values recorded show that only the relationship between the flare stack height and the ($\delta LST_{60\text{-}450m}$)$_W$ give statistically significant result. For Julian day, and each of the ($\delta LST_{60\text{-}450m}$)$_N$, ($\delta LST_{60\text{-}450m}$)$_E$, ($\delta LST_{60\text{-}450m}$)$_S$ and ($\delta LST_{60\text{-}450m}$)$_W$, statistically insignificant results and positive correlation were recorded. Furthermore, the relationship between Month and the ($\delta LST_{60\text{-}450m}$)$_N$, ($\delta LST_{60\text{-}450m}$)$_E$, ($\delta LST_{60\text{-}450m}$)$_S$ and ($\delta LST_{60\text{-}450m}$)$_W$ give statistically insignificant results but positive correlation. Finally, results obtained from the relationship between Year and each of the ($\delta LST_{60\text{-}450m}$)$_N$ and the ($\delta LST_{60\text{-}450m}$)$_W$ show positive correlation. However, the relationship between Year and ($\delta LST_{60\text{-}450m}$)$_E$ and ($\delta LST_{60\text{-}450m}$)$_S$ show negative correlation. All relationships give statistically insignificant results. The results presented in Table 19, is similar to that of Table 18 except the relationship between the flare stack height and the ($\delta LST_{60\text{-}450m}$)$_S$, and Year and ($\delta LST_{60\text{-}450m}$)$_N$ that show negative correlation. In Table 20, East direction show the highest value of 35.8 K, followed by North with 34.9 K, and the West has 31.3 K. The South direction recorded the lowest value of 27.9 K which

suggests that the effect of the South prevailing wind in the Niger Delta (Morakinyo et al., 2022) could be the reason for the results. The wind blew from the South, directed more towards the East direction, followed by the North and the West directions.

From the multiple linear regression analysis, the $r^2 = 0.05$ obtained from (Eq. 11 and Eq. 12) show that only 5 % of the variability in the $(\delta LST_{60\text{-}450m})_N$ and the $(\delta LST_{60\text{-}450m})_E$ were explained by the variables examined; and are accounted for in the resulting relationship. Vegetation density, vegetation types, volume of the burning gas, rate of the burning gas etc are some of the factors that would account for the unexplained variability.

The impact of the 3 available variables considered on the change in the LST ($\delta LST_{60\text{-}450m}$) retrieved at the 11 flaring sites in Nigeria have been assessed. Facility size in the N, E, S and W directions, and height of the flare stack in the West direction gives significant results. However, their correlation is negative. Firstly, the 2 largest facilities are Umurolu (4 flare stacks) and Bonny LNG (5 flare stacks) with inland and coastal sites respectively show similar results. This suggests that the facility size and the number of flare stack on each facility contributed to the results. Secondly, the medium and small sizes inland flow stations investigated are Alua, Rukpokwu, Obigbo and Chokocho. The acquired results show that the impact of the facility size on ($\delta LST_{60\text{-}450m}$) is statistically significant, which suggest that the volume of the burning gas is large, and the rate at which the gas is burning is quite high at these facilities. Sara is a coastal oil well facility with limited size, rough terrain, and connected with several pipes. However, the enormity of the recorded ($\delta LST_{60\text{-}450m}$) suggested that the oil well is performing at a high capacity with large volume and high rate of the burning gas. Eleme I and II refineries are large facilities with one flare stack at each refinery; and their results show a non-significant impact. This suggests that the effect of a single flare stack at both refineries, and damaged to them in 1988 has affected the results. Since 1988, their usage and production capacity has been reduced to between (15-25) % (Ogbuigwe, 2018). Furthermore, the results from the multiple linear regression analysis also supported the ANOVA results by showing that the facility size may exert a negative influence on ($\delta LST_{60\text{-}450m}$). However, the overall percentage of variability explained by the 3 variables is low.

Conclusion

Landsat data used for this study covered a period of 38 years, which is good enough to give reliable indisputable results. From the pairwise linear regression analysis, the research showed that the facility size in the N, E, S and W directions, and the flare stack height in the West direction have significant results on the ($\delta LST_{60\text{-}450m}$). Also, the results from multiple regression analysis show that $r^2 = 0.05$. From these results, it can be concluded that the facility size, flare stack height and time contributed only 5 % to the ($\delta LST_{60\text{-}450m}$). Major limitations encountered in this research include lack of data on the volume and the rate of the burning gas. This requires further research to enable the author to draw firm conclusions about what exactly drives ($\delta LST_{60\text{-}450m}$). Hence, the following recommendations are made: The enforcement of the multi-national oil companies in Nigeria to release information on all activities regarding oil and gas exploration and exploitation to the general public especially to the stakeholders, organizations, educational and research institutions involved in the oil and gas business through appropriate and standard policies must be carried out by the Nigerian Government. Finally, the insecurity issue in Nigeria is a very big challenge that hinders accessibility to the oil and gas facilities; and also causes vandalization of these facilities. Nigerian Government needs to find a lasting solution to this problem in order to have a safe and peaceful country.

References

Anastasios, P., Theleia, M., & Constantinos, C. (2018). Quantifying the trends in land surface temperature and surface urban heat island intensity in mediterranean cities in view of smart urbanization. *Urban Science* 2(16).

Barsi, J. A., Schott, J. R., Palluconi, F. D., & Hook, S. J. (2005). Validation of a web-based atmospheric correction tool for single thermal band instruments, Proceding. SPIE, vol. 5882, Bellingham, WA. 7.

Bechtel, B. A. (2015). New global climatology of annual land surface temperature. *Remote Sensing* 7: 2850-2870.

Berk, A., Anderson, G. P., & Acharya et al. P. K. (1999). MODTRAN4 User's Manual, Air Force Research Laboratory, Ontar Corporation, North Andover, MA, USA 10-35.

Caseiro, A., Gehrke, B., Rücker, G., Leimbach, D., & Kaiser, J. W. (2020). Gas flaring activity and black carbon emissions in 2017 derived from Sentinel-3A SLSTR. *Earth System Science Data* 12(3): 2137-2155.

Chander, G., & Markham, K. (2003). Revised Landsat-5 TM radiometric calibration procedures and post-calibration dynamic ranges. *IEEE Transactions on Geosciences and Remote Sensing* 41(11): 2674-2677.

Chapin, F., Sturm, M., Serreze, M., McFadden, J., Key, J., Lloyd, A., McGuire, A., Rupp, T., Lynch, A., & Schimel, J. (2005). Role of land surface changes in Arctic summer warming. *Science* 310: 657-660.

Dung, E. J., Bombom, L. S., & Agusomu, T. D. (2008). The effects of gas flaring on crops in the Niger Delta, Nigeria. *GeoJournal* 73: 297-305.

Edu, A. (2021). Gas flares, oil spills worsen climate change in the Niger Delta communities. *Guardian*. From https://guardian.ng/property/gas-flares-oil-spills-worsen-climate-change-in-niger-delta-communities/. Retrieved 18 October 2021.

Elvidge, C. D., Zhizhin, M., Baugh, K., Hsu, F. C., & Ghosh, T. (2016). Methods for global survey of natural gas flaring from Visible Infrared Imaging Radiometer Suite data. *Energies* 9(14).

Elvidge, C. D., Zhizhin, M., Hsu, F. C., & Baugh, K. E. (2013). VIIRS Nightfire: Satellite pyrometry at night. *Remote Sensing*, 5: 4423-4449.

ESRI (2022). Map of Africa showing Nigeria.

Google Earth (2022). Location of Rivers State in the Niger Delta, Nigeria; and the 11 flaring sites studied in Rivers State, Nigeria.

Isichei, A. O., & Sandford, W. W. (1976). The Effects of Waste Gas Flares on the Surrounding Vegetation of South-Eastern Nigeria. *Applied Ecology* 13: 177-187.

Kerr, Y. H., Lagouarde, J. P., Nerry, F., Ottlé, C., Quattrochi, D. A., & Luvall, J. C. (2000). Land surface temperature retrieval techniques and applications. *Thermal Remote Sensing* 33-109.

Li, Z., Tang, B., Wu, H., Ren, H., Yan, G., Wan, Z., Trigo, I. F., & Sobrino, J. A. (2013). Satellite-derived land surface temperature: Current status and perspectives. *Remote Sensing of Environment* 131: 14-37.

Liu, Y., Hu, C., Zhan, W., Sun, C., Murch, B., & Ma, L. (2018). Identifying industrial heat sources using time-series of the VIIRS Nightfire product with an object-oriented approach. *Remote Sensing of Environment* 204: 347-365.

Maaharjan, A. (2018). Land use/Land cover of Katnmandu valley by using remote sensing and GIS (M.Sc. dissertation). Tribhuvan University, Kirtipur, Kathmandu, Nepal.

Morakinyo, B. O., Lavender, S., & Abbott, V. (2022). Investigation of potential prevailing wind impact on land surface temperature at gas flaring sites in the Niger Delta, Nigeria, *International Journal of Environment and Geoinformatics (IJEGEO)*, 9(1):179-190.

Morakinyo, B. O., Lavender, S., & Abbott, V. (2021). The methodology and results from ground validation of satellite observations at gas flaring sites in Nigeria. *International Journal of Environment and Geoinformatics (IJEGEO)*, 8(3): 290-300.

Morakinyo, B. O., Lavender, S., & Abbott, V. (2020). Retrieval of land surface temperature from earth observation satellites for gas flaring sites in the Niger Delta, Nigeria. *International Journal of Environmental Monitoring and Analysis* 8 (3): 59-74.

Morakinyo, B. O., Lavender, S., Schwarz, J., & Abbott, V. (2019). Mapping of land cover and estimation of their emissivity values for gas flaring sites in the Niger Delta. *British Journal of Environmental Sciences,* 7(2): 31-58.

Morakinyo, B. O. (2015). Flaring and pollution detection in the Niger Delta using remote sensing. Ph.D Thesis, School of Marine Science and Engineering, University of Plymouth, Plymouth, United Kingdom.

Ogbuigwe, A. (2018). Refining in Nigeria: History, challenges and prospects. *Applied Petrochemical Research* 8: 181-192.

Qin, Q., Zhang, N., Nan, P., & Chai, L. (2011). Geothermal area detection using Landsat ETM+ thermal infrared data and its mechanistic analysis: A case study in Tengchong, China. *International Journal of Applied Earth Observation and GeoInformation* 13: 552-559.

Song, Z., Li, R., Qiu, R., Liu, S., Tan, C., Li, Q., Ge, W., Han, X., Tang, X., Shi, W., Song, L., Yu, W., Yang, H., & Ma, M. (2018a). Global land surface temperature influenced by vegetation cover and PM 2.5 from 2001 to 2016. *Remote Sensing* 10: 2034.

Song, L., Liu, S., Kustas, W. P. Nieto, H. Sun, L., Xu, Z., Skaggs, T. H., Yang, Y., Ma, M., & Xu, T. (2018b). Monitoring and validating spatially and temporally continuous daily evaporation and transpiration at river basin scale. *Remote Sensing of Environment* 219: 72-88.

Sun, L., Sun, R., Li, X., Chen, H., & Zhang, X. (2011). Estimating evapotranspiration using improved fractional vegetation cover and land surface temperature space. *Journal of Resource Ecology* 2: 225-231.

Ubani, E. C., & Onyejekwe, I. M. (2013). Environmental impact analyses of gas flaring in the Niger Delta region of Nigeria. *American Journal of Scientific and Industrial Research* 4(2): 246-252.

USGS (2022). Landsat 8 specifications. From https://www.satimagingcorp.com/satellite-sensors/other-satellite-sensors/landsat-8/. Retrieved 22 April 2022.

Yuan, F., & Bauer, M. E. (2007). Comparison of impervious surface area and normalized difference vegetation index as indicators of surface urban heat island effects in Landsat imagery. Remote Sensing of Environment 106: 375-386.

Zhang, X., Scheving, B., Shoghli, B., Zygarlicke, C., & Wocken, C. (2015). Quantifying gas flaring CH4 consumption using VIIRS. *Remote Sensing* 7: 9529-9541.

Zhang, Y., Odeh, I., & Han, C. (2009). Bi-temporal characterization of land surface temperature in relation to impervious surface area, NDVI and NDBI, using a sub-pixel image analysis. *International Journal of Applied Earth Observation and Geoinformation* 11: 256-264.

Zhao, L., Yang, Z.-L., & Hoar, T. J. (2016). Global soil moisture estimation by assimilating AMSR-E brightness temperatures in a coupled CLM4-RTM-DART system. *Journal of Hydrometeorology* 17: 2431-2454.